

# SCIENTIFIC REPORTS



OPEN

## Polarization-independent, wide-incident-angle and dual-band perfect absorption, based on near-field coupling in a symmetric metamaterial

Bui Son Tung<sup>1</sup>, Bui Xuan Khuyen<sup>1</sup>, Young Ju Kim<sup>1</sup>, Vu Dinh Lam<sup>2</sup>, Ki Won Kim<sup>3</sup> & YoungPak Lee<sup>1</sup>

We numerically and experimentally investigated a dual-band metamaterial perfect absorber (MPA), utilizing the near-field coupling of double split-ring resonators (DSRRs). Owing to the near-field coupling between resonators, two arms in each DSRR resonate in different phases, leading to a dual-band perfect absorption. The proposed MPA also exhibits polarization-insensitive behavior and maintains the high absorption above 90% up to a wide range of incident angle more than 45°. Finally, to further consolidate our approach, a multi-band absorption is also studied by exploiting the near-field coupling among a larger number of DSRRs. Our work is expected to be applied to future broadband devices using MPA.

Metamaterial perfect absorbers (MPAs) have drawn much attention in science society due to potential applications in energy harvester<sup>1</sup>, bio-sensor<sup>2</sup>, subwavelength resolution<sup>3</sup>, photovoltaics<sup>4</sup>, emitter<sup>5</sup>, detector<sup>6</sup> and modulator<sup>7</sup>. Since the first demonstration of MPA in 2008<sup>8</sup>, many MPAs have been demonstrated in different regions such as MHz<sup>9,10</sup>, GHz<sup>11,12</sup>, THz<sup>13,14</sup>, infrared<sup>15,16</sup> and optical<sup>17,18</sup> frequencies. For real applications and devices, a broad bandwidth is highly preferred, making multi-band and broadband MPAs one of the main research directions. Although several approaches have been developed for multi-band and broadband absorption so far, specific obstacles still exist. Resistor-integrated MPAs<sup>19</sup> exploit the loss of resistor to broaden the resonance bandwidth, but the operational frequencies are limited to low frequencies (below GHz) due to the size of resistors. Multi-layer stacking<sup>20</sup>, where different layers yield their own resonance frequencies, is also a way to create multi-band and broadband MPAs. However, the thickness is much increased making the MPA hard to be applied in ultrathin devices. Another similar way is combining many resonators<sup>21</sup>, which share a same design but have small deviations in the geometrical size, to exhibit closely separate resonances in the plane of structure. Unfortunately, in order to be broadband, the deviations of geometrical size should be small enough, which might be impossible for fabrication, especially, in the optical region.

Recently, the near-field coupling in metamaterial (MM), which is famous for electromagnetically-induced transparency (EIT)<sup>22,23</sup>, has been exploited as a different way to obtain multi-band absorption because the MPA structures do not suffer from the problem of size deviations in the combined-resonator method<sup>24–26</sup>. However, to induce an EIT-like effect for multi-band absorption, an asymmetry of structure should be devised, making the MPA strongly polarization-sensitive. In this report, we propose another approach to create multi-band absorption, based on the near-field coupling in a symmetric MM structure. By exploiting the near-field coupling of identical resonators, the dual-band and the multi-band absorption can be induced. Differently from the mentioned works, the coupling occurs in a symmetric structural design instead of an asymmetric one, for the MPA to be polarization-insensitive. The proposed absorber is not only polarization-insensitive but works for a wide range of incident angle, which is useful for real applications.

<sup>1</sup>Hanyang University, Department of Physics and RINS, Seoul, 04763, Korea. <sup>2</sup>Institute of Materials Science, Vietnam Academy of Science and Technology, Hanoi, Vietnam. <sup>3</sup>Sunmoon University, Asan, 31460, Korea. Correspondence and requests for materials should be addressed to Y.L. (email: [yplee@hanyang.ac.kr](mailto:yplee@hanyang.ac.kr))

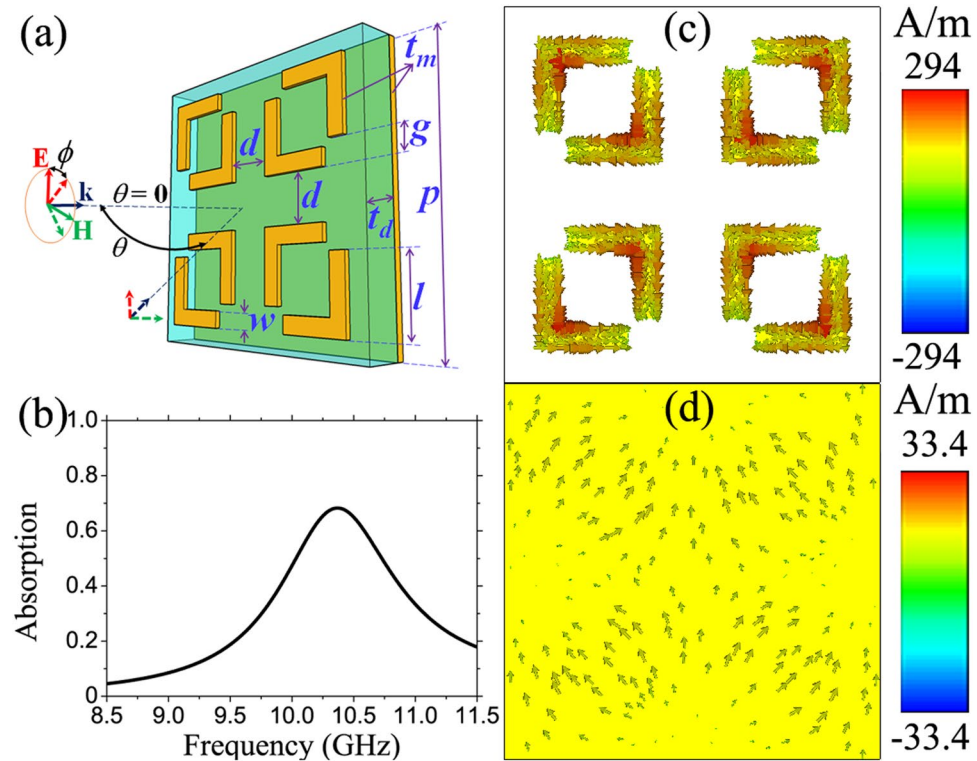


**Figure 1.** (a) Illustration of the unit cell of MPA with the polarization of electromagnetic wave. (b) Absorption spectrum of the MPA. Surface currents on (c) the front patterned and (d) the continuous back metallic layers.

## Results

**Design of structure.** Figure 1(a) presents an illustrated unit cell of our proposed MPA structure, which is composed of a front patterned metallic layer, a middle dielectric spacer and a back metallic film. Copper is chosen as the metal with a conductivity of  $5.96 \times 10^7$  S/m, while the dielectric layer is made of FR-4 with a dielectric constant of 4.3 and a loss tangent of 0.025. The thicknesses of metallic layers and dielectric spacer are  $t_m = 0.035$  and  $t_d = 1.6$  mm, respectively. The patterned metallic structure consists of four identical double split-ring resonators (DSRRs), which are rotated by  $90^\circ$  in turn to make a symmetric MPA structure and separated from each other by a distance  $d = 3.5$  mm. The arms of DSRR have a side length  $l = 4.5$  mm and a width  $w = 1$  mm and the gap between these arms is  $g = 1.5$  mm. The whole MPA is a periodic array of the unit cell with a periodicity  $p = 19$  mm. The incident electromagnetic (EM) wave is normal to the MPA plane with electric (**E**) and magnetic (**H**) fields are polarized along the arm lengths and are perpendicular to each other. Figure 1(b) is the simulated absorption spectrum of proposed MPA structure. Because the left and the right DSRRs are mirror-symmetric with respect to the **E** direction, the responses of four rings are identical. Therefore, only one absorption peak is observed at 10.3 GHz with an absorption of 68.2%. The surface currents in Figs 1(c) and (d) reveal that the absorption results from a magnetic resonance, indicated by the anti-parallel currents on the front and the back metallic layers.

### Dual-band metamaterial absorber, based on near-field coupling: fabrication and characterization.

Next, an approach to make a dual-band MPA, based on the near-field coupling, is demonstrated. Figures 2(a) and (b) show a fabricated sample and the measurement configuration, respectively. Four samples with the distance  $d$  varied from 3.5 to 0.5 mm were fabricated by using the traditional printed-circuit board, followed by the photolithography process. Because there is no transmission through MPA due to the back metal film, only the reflection measurement is set up. The absorption is calculated as  $A(\omega) = 1 - |S_{11}(\omega)|^2$ , where  $S_{11}(\omega)$  is the reflection parameters. The simulated and the measured absorption spectra according to  $d$  are given in Figs 2(c) and (d), respectively, which show a good agreement between them. Initially, when the DSRRs are far from each other, there is only one absorption peak as demonstrated above. When the separation between rings are smaller, the near-field interaction between them is considerable and stronger. Therefore, the shape of absorption spectrum is gradually distorted, becomes asymmetric and, finally, the initial peak splits clearly into two absorption peaks for  $d = 0.5$  mm. The absorption peaks are located at 9.7 and 10.3 GHz, both with an absorption of 97.1%.

The impedance spectra of MPAs for  $d = 3.5$  and  $d = 0.5$  mm are presented in Fig. 3. The impedance of MPA is calculated using the expression below<sup>27</sup>:

$$Z(\omega) = \sqrt{\frac{(1 + S_{11}(\omega))^2 - S_{21}(\omega)^2}{(1 - S_{11}(\omega))^2 - S_{21}(\omega)^2}} \quad (1)$$

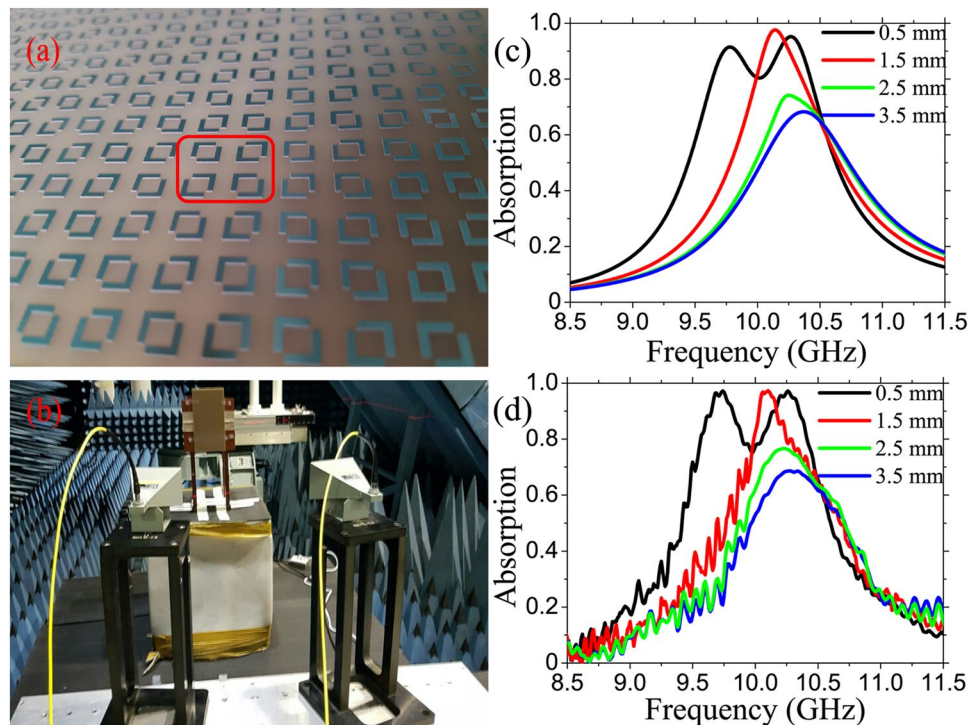


**Figure 2.** (a) A fabricated MPA sample, the red box indicates the unit cell of structure. (b) Measurement configuration. (c) Simulated and (d) experimental absorption spectra according to separation  $d$  of DSRRs.

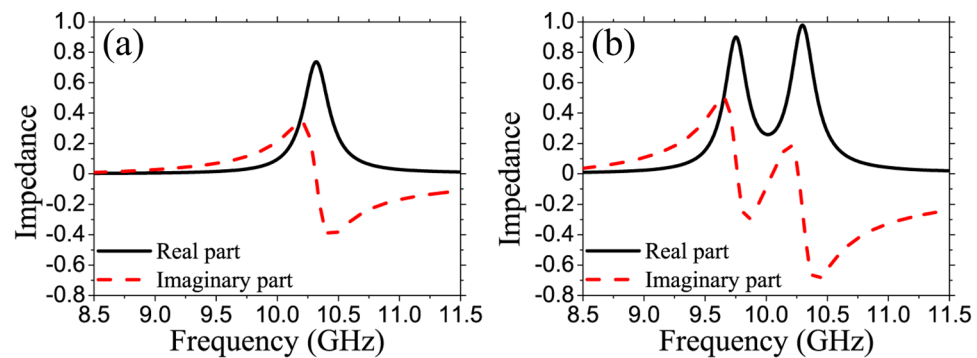


**Figure 3.** Real and imaginary parts of impedance for (a)  $d = 3.5$  and (b)  $d = 0.5$  mm.

The results clarify that the impedance of MPA at two frequencies 9.7 and 10.3 GHz matches well with that of the air for  $d = 0.5$  mm. Therefore, the reflection is minimized at these frequencies. Combining with the transmission block by the back metal, consequently, two near-perfect absorption peaks are observed as in Fig. 2. Furthermore, as shown in Fig. 3(a), the impedance spectrum of MPA only have one peak and it is not really well matched, which explains why the absorption is low for  $d = 3.5$  mm.

To understand better the nature behind the observed phenomena, the surface currents on the front patterned metallic layer are presented at two absorption frequencies, as shown in Fig. 4. Differently from Fig. 1(c) when  $d = 3.5$  mm, two arms of DSRRs do not exhibit the same behavior. The induced currents on inner arms are maximized while those on outer arms are nearly minimized at the first resonance [Fig. 4(a)]. On the other hand, at the second resonance, the maximum and the minimum currents are observed on the outer and the inner arms, respectively. In addition, the induced currents on DSRRs are anti-parallel at the two resonance frequencies. Furthermore, at both resonance frequencies, the directions of currents on two arms of individual DSRR are also opposite. These results indicate that the near-field coupling between DSRRs induces highly contrastive states not only between two resonance frequencies but between two arms of individual DSRR at a same resonance frequency. In the attached Supplementary Information, the near-field coupling between DSRRs is described further by the radiating two-oscillator model<sup>28</sup> for a simplified structure, in which the back metal layer of MPA is removed.

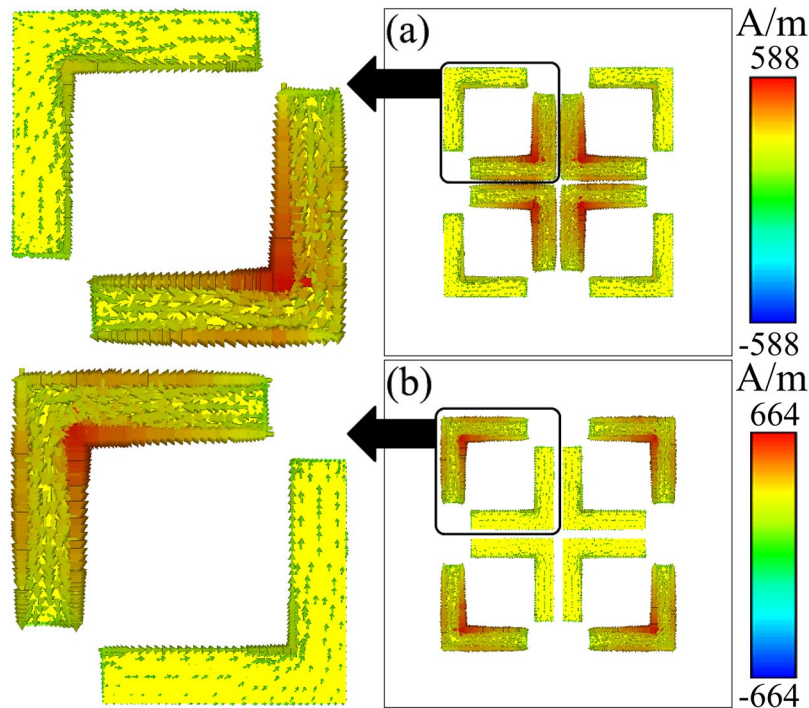


**Figure 4.** Surface currents on the front patterned metallic layer at (a) 9.7 and (b) 10.3 GHz when  $d = 0.5$  mm. The black boxes and arrows indicate the magnified areas.

To evaluate further the real applicability of MPA, the dependences of polarization and incident angle of EM wave are investigated. As shown in Fig. 5(a), the simulated absorption spectrum of MPA is independent of the polarization state at the normal incidence. The polarization insensitivity of MPA is achieved due to the symmetric geometry of structural design. Figures 5(b) and (c) present the simulated and experimental absorption spectra according to incident angle. Both results are in quite good agreement. The dual-band absorption is maintained above 90% in a wide range of incident angle ( $\theta > 45^\circ$ ). At  $\theta = 60^\circ$ , the absorption starts reducing to be 90% and 85% for the first and the second peaks, respectively. It is also shown that the frequency interval between two absorption peaks is slightly larger by increasing the incident angle. The observed phenomenon might be explained, based on the near-field coupling between resonators. When the incidence is not normal to the structural plane, the MPA structure can be considered to be asymmetric with respect to the EM wave<sup>29,30</sup>. The asymmetric factor also contributes to the near-field coupling between resonators, making the coupling strength stronger. Consequently, the two split resonances are separated further at larger incident angle.

Finally, to consolidate our proposed approach, an extended structure is presented and compared with the dual-band MPA structure. The extended structure exploits the near-field coupling of a larger number of resonators ( $4 \times 4$  DSRRs) than that of the dual-band MPA structure ( $2 \times 2$  DSRRs). As shown in Fig. 6, the simulated absorption spectrum of  $4 \times 4$  DSRRs structure is broader and more efficient than that of  $2 \times 2$  DSRRs structure. Instead of the dual-band absorption, the improved MPA exhibits a multi-band absorption (four obviously-observable peaks at least) with the bandwidth at 80% absorption is broader by 37%. Especially, a broadband absorption region, whose absorption is over 90%, is obtained with a bandwidth of 0.5 GHz.

## Discussion

In summary, we demonstrated an approach to make a dual-band MPA by making use of the near-field coupling in a symmetric structure. Both simulated and experimental results show transformation of the absorption spectrum from single- to dual-band absorption by adjusting the separation of DSRRs. The mechanism is clarified to be the near-field coupling, which makes the MPA behave differently at two resonance frequencies, and the inner and the outer arms of DSRRs exhibit opposite behaviors even at the same resonance frequency. The proposed dual-band MPA is also polarization-insensitive and able to operate in a wide range of incident angle. Finally, by extending the number of coupled resonators, we presented that the absorption could be improved to be broader and more efficient. Our work contributes another way to provide broadband MPAs, which might be useful in various future applications.

## Methods

**Simulation.** In our work, the simulation was performed by using a finite-integration package (CST Microwave Studio<sup>31</sup>). The unit-cell boundary was applied along two orthogonal directions on the plane of structure. The polarization of electromagnetic wave was chosen as in Fig. 1(a).

**Fabrication.** The fabrication was done using the conventional printed-circuit-board method. A FR-4 substrate of 1.6 mm thickness was sandwiched between 0.035 mm-thick copper layers, one of which is coated by



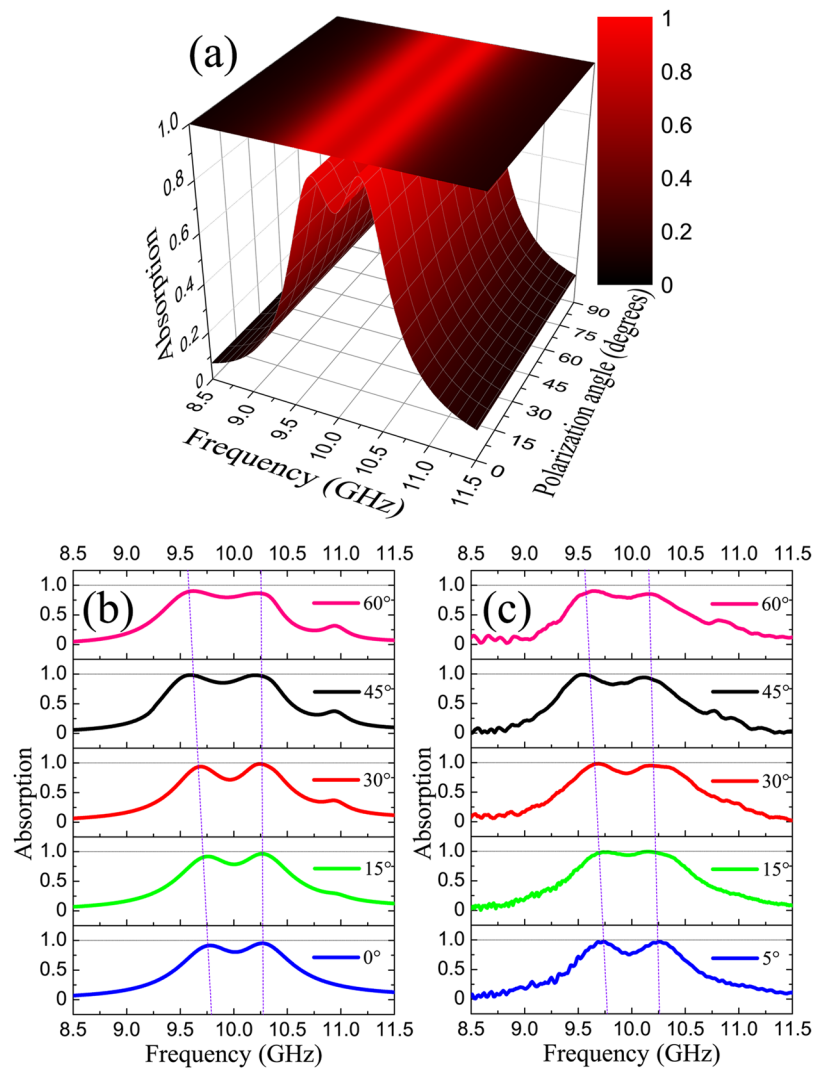


**Figure 5.** (a) Simulated absorption spectra according to polarization angle. Dependence of (b) simulated and (c) experimental absorption spectra on the incident angle  $\theta$  of EM wave.

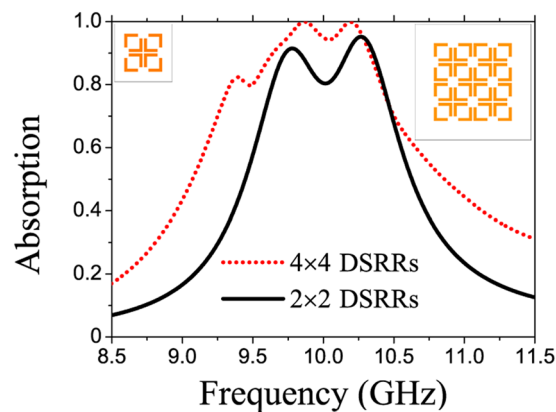


**Figure 6.** Comparison of the simulated absorption spectra between two MPAs with the unit cells of  $2 \times 2$  (left inset) and  $4 \times 4$  (right inset) DSRRs. The periodicity of  $4 \times 4$  DSRR structure is 38 mm, which is as twice as that of the  $2 \times 2$  DSRR structure.

photoresist. After putting a mask, which has the design of structure, on one side of sample, the photolithography process was carried out. Then, the exposed part of the copper film was removed by the wet-etching technique, giving the structural pattern.

**Measurement.** The measurement was carried out in a microwave anechoic chamber using a Hewlett-Packard E8362B network analyzer connected to linearly-polarized microwave standard-gain horn antennas. In order to fulfill the far-field condition, the distance between antennas and sample was set to be 2.0 m, which is around 66 times larger than the absorption wavelength.

## References

- Almoneef, T. S. & Ramahi, O. M. Metamaterial electromagnetic energy harvester with near unity efficiency. *Appl. Phys. Lett.* **106**, 153902 (2015).
- Ishikawa, A. & Tanaka, T. Metamaterial absorbers for infrared detection of molecular self-assembled monolayers. *Sci. Rep.* **5**, 12570 (2015).
- Xie, Y. *et al.* A subwavelength resolution microwave/6.3 GHz camera based on a metamaterial absorber. *Sci. Rep.* **7**, 40490 (2017).
- Coppens, Z. J., Kravchenko, I. I. & Valentine, J. G. Lithography-free large-area metamaterials for stable thermophotovoltaic energy conversion. *Adv. Opt. Mater.* **4**, 671–676 (2016).
- Liu, X. *et al.* Taming the blackbody with infrared metamaterials as selective thermal emitters. *Phys. Rev. Lett.* **107**, 045901 (2011).
- Li, W. & Valentine, J. Metamaterial perfect absorber based hot electron photodetection. *Nano Lett.* **14**, 3510–3514 (2014).
- Savo, S., Shrekenhamer, D. & Padilla, W. J. Liquid crystal metamaterial absorber spatial light modulator for THz applications. *Adv. Opt. Mater.* **2**, 275–279 (2014).
- Landy, N. I., Sajuyigbe, S., Mock, J. J., Smith, D. R. & Padilla, W. J. Perfect metamaterial absorber. *Phys. Rev. Lett.* **100**, 207402 (2008).
- Khuyen, B. X. *et al.* Ultrathin metamaterial-based perfect absorbers for VHF and THz bands. *Curr. Appl. Phys.* **16**, 1009–1014 (2016).
- Khuyen, B. X. *et al.* Miniaturization for ultrathin metamaterial perfect absorber in the VHF band. *Sci. Rep.* **7**, 45151 (2017).
- Ding, F., Cui, Y., Ge, X., Jin, Y. & He, S. Ultra-broadband microwave metamaterial absorber. *Appl. Phys. Lett.* **100**, 103506 (2012).
- Zhang, Y., Duan, J., Zhang, B., Zhang, W. & Wang, W. A flexible metamaterial absorber with four bands and two resonators. *J. Alloys Compd.* **705**, 262–268 (2017).
- Tao, H. *et al.* Highly flexible wide angle of incidence terahertz metamaterial absorber: Design, fabrication, and characterization. *Phys. Rev. B* **78**, 241103 (2008).
- Wang, W., Wang, K., Yang, Z. & Liu, J. Experimental demonstration of an ultra-flexible metamaterial absorber and its application in sensing. *J. Phys. D: Appl. Phys.* **50**, 135108 (2017).
- Liu, X., Starr, T., Starr, A. F. & Padilla, W. J. Infrared spatial and frequency selective metamaterial with near-unity absorbance. *Phys. Rev. Lett.* **104**, 207403 (2010).
- Hasan, D. *et al.* Novel CMOS-compatible Mo<sub>2</sub>Al<sub>2</sub>N<sub>3</sub>Mo platform for metamaterial-based mid-ir absorber. *ACS Photonics* **4**, 302–315 (2017).
- Hao, J. *et al.* High performance optical absorber based on a plasmonic metamaterial. *Appl. Phys. Lett.* **96**, 251104 (2010).
- Wang, W. *et al.* Broadband optical absorption based on single-sized metal-dielectric-metal plasmonic nanostructures with high- $\epsilon''$  metals. *Appl. Phys. Lett.* **110**, 101101 (2017).
- Ye, D. *et al.* Ultrawideband dispersion control of a metamaterial surface for perfectly-matched-layer-like absorption. *Phys. Rev. Lett.* **111**, 187402 (2013).
- Kim, Y. J. *et al.* Dual broadband metamaterial absorber. *Opt. Express* **23**, 3861–3868 (2015).
- Ma, W., Wen, Y. & Yu, X. Broadband metamaterial absorber at mid-infrared using multiplexed cross resonators. *Opt. Express* **21**, 30724–30730 (2013).
- Zhang, S., Genov, D. A., Wang, Y., Liu, M. & Zhang, X. Plasmon-induced transparency in metamaterials. *Phys. Rev. Lett.* **101**, 047401 (2008).
- Han, S., Cong, L., Gao, F., Singh, R. & Yang, H. Observation of fano resonance and classical analog of electromagnetically induced transparency in toroidal metamaterials. *Ann. Phys. (Berlin)* **528**, 352–357 (2016).
- Tung, B. S. *et al.* Multi-band near-perfect absorption via the resonance excitation of dark meta-molecules. *Opt. Commun.* **356**, 362–367 (2015).
- Dung, N. V. *et al.* Simple metamaterial structure enabling triple-band perfect absorber. *J. Phys. D: Appl. Phys.* **48**, 375103 (2015).
- Liu, Y., Zhang, Y. Q., Jin, X. R., Zhang, S. & Lee, Y. P. Dual-band infrared perfect absorber for plasmonic sensor based on the electromagnetically induced reflection-like effect. *Opt. Commun.* **371**, 173–177 (2016).
- Chen, X., Grzegorzczak, T. M., Wu, B.-I., Pacheco, J. & Kong, J. A. Robust method to retrieve the constitutive effective parameters of metamaterials. *Phys. Rev. E* **70**, 016608 (2004).
- Tassin, P. *et al.* Electromagnetically induced transparency and absorption in metamaterials: the radiating two-oscillator model and its experimental confirmation. *Phys. Rev. Lett.* **109**, 187401 (2012).
- Jin, X.-R. *et al.* Manipulation of electromagnetically-induced transparency in planar metamaterials based on phase coupling. *J. Appl. Phys.* **111**, 073101 (2012).
- Aksyuk, V., Lahiri, B., Holland, G. & Centrone, A. Near-field asymmetries in plasmonic resonators. *Nanoscale* **7**, 3634–3644 (2015).
- CST of America, Inc., 492 Old Connecticut Path, Suite 505, Framingham, MA 01701, USA. <http://www.cst.com>.

## Acknowledgements

This work was supported by Institute for Information & communications Technology Promotion (IITP) grant funded by the Korea government (MSIT) (No. 2013-0-00375) and by the NRF funded by MSIT, Korea (No. 2017R1A2B4003916).

## Author Contributions

B.S. Tung, V.D. Lam, K.W. Kim and Y.P. Lee conceived the idea. B.X. Khuyen and Y.J. Kim fabricated the samples. The simulation was carried out by B.S. Tung and B.X. Khuyen. The measurement was performed by B.S. Tung and Y.J. Kim. B.S. Tung and Y.P. Lee did the analysis and wrote the manuscript. All the authors discussed and commented on the manuscript.

## Additional Information

**Supplementary information** accompanies this paper at doi:[10.1038/s41598-017-11824-7](https://doi.org/10.1038/s41598-017-11824-7)

**Competing Interests:** The authors declare that they have no competing interests.

**Publisher's note:** Springer Nature remains neutral with regard to jurisdictional claims in published maps and institutional affiliations.



**Open Access** This article is licensed under a Creative Commons Attribution 4.0 International License, which permits use, sharing, adaptation, distribution and reproduction in any medium or format, as long as you give appropriate credit to the original author(s) and the source, provide a link to the Creative Commons license, and indicate if changes were made. The images or other third party material in this article are included in the article's Creative Commons license, unless indicated otherwise in a credit line to the material. If material is not included in the article's Creative Commons license and your intended use is not permitted by statutory regulation or exceeds the permitted use, you will need to obtain permission directly from the copyright holder. To view a copy of this license, visit <http://creativecommons.org/licenses/by/4.0/>.

© The Author(s) 2017